International Journal of Modern Manufacturing Technologies
ISSN 2067–3604, Vol. XII, No. 1 / 2020

FINITE ELEMENT MODELING BASED MATERIAL REMOVAL ANALYSIS OF NON-CONDUCTIVE MATERIALS IN ECDM USING ADAPTIVE TOOL FEED SYSTEM

Viveksheel Rajput, Mudimallana Goud, Narendra Mohan Suri

Department of Production and Industrial Engineering, PEC, Chandigarh, India, 160012

Corresponding author: Viveksheel Rajput, sheelrajput03@gmail.Com

Abstract: Electro-Chemical Discharge Machining (ECDM) is a hybrid process for machining "non-conductive" and "difficult-to-cut" materials such as glass, quartz, ceramics, etc. These materials exhibit diverse applications in the fields of Micro-electro-mechanical systems (MEMS) and lab on chips such as micro-sensors, micro-pumps, micro-accelerometer. ECDM successfully fabricates micro-features on these materials with higher geometrical tolerances. It involves the removal mechanism of Electro-Discharge Machining (EDM) and Electro-chemical Machining (ECM) processes simultaneously. However, a limited number of studies were reported in the analytical analysis of material removal of different non-conductive materials. This paper develops a FEM based thermal model to compare the removal rate of glass, quartz, and alumina (Al_2O_3) under similar working conditions. Temperature plots are utilized to estimate the material removal of different work materials. Predicted results are validated by comparing it with the previously reported simulation and experimental results. Experiments are also performed to validate the current study using the adaptive tool feed control system in ECDM. A good agreement is observed between the predicted and experimental results. It was observed that the material removal rate increases with the increase in applied concentration and applied voltage. An increase of 3.53 and 10.13mg/min in MRR was observed in a soda-lime glass when compared to quartz and alumina at 60 wt% NaOH concentration.

Key words: Finite element modeling, ECDM, Spark radius, Gaussian heat, Applied voltage, Material removal rate, Cracks).

1. INTRODUCTION

The micro-machining of non-conductive materials such as glass, quartz, etc. is difficult to achieve owing to their brittleness. Glass and quartz are high in demand in the field of MEMS, medical and aviation due to their unique properties. They have good transparency, resistance to chemicals, and high hardness [1, 2]. Alumina is an advanced material that exhibits high hardness, high strength to weight ratio and higher corrosion resistance, etc. They are widely used in advanced engineering applications such as aerospace, automotive brakes, piezoceramic sensors and biomedical implants due to excellent biocompatibility [3, 4]. These materials (glass, quartz, and alumina) are strenuous to process by conventional machining methods because of cutting forces. It destroys the material properties and results in its failure. Thus, a high challenge lies in the machining of these materials which are non-conductive as well as brittle and hard. It was earlier reported that other techniques can be employed to machine these materials such as electric discharge machining (EDM), Ultrasonic machining (USM) and Laser beam machining (LBM), etc [5, 6]. Besides, these machining methods result in the poor surface finish (SF), high heat-affected zone (HAZ), high tool wear, etc [7, 8]. ECDM process is developed in lieu of overcoming these limitations. It is known as the triumph process for machining these materials by blending the discharge-based machining (EDM) and chemical-based machining (ECM) simultaneously. The material removal in ECDM is the result of thermal erosion due to the Joule heating of the work material. Chemical dissolution also results in the removal of the material. The combined material removal phenomena of ECM and EDM produce larger removal of the material when compared to individual ECM or EDM process. It has successfully demonstrated the processing of non-conducive work materials with micro-features [9, 10]. ECDM was firstly demonstrated by Kurafuji in 1968 during glass drilling through electric discharges [11]. The schematic diagram for illustrating the working principle of the ECDM process is shown in Figure 1. The non-conductive work material which is to be machined is immersed in an aqueous solution of an electrolyte (generally NaOH or KOH). A constant or pulsed voltage across the tool electrode (cathode) and auxiliary electrode (anode) are applied. Both the electrodes are kept at a distance of few centimetres (defined as an inter-electrode gap, IEG). The tool electrode is partially immersed inside the electrolyte (known as machining gap). The surface area of the tool electrode is thin as compared to the auxiliary electrode. It was reported that high current densities are produced at the thin edges of the tool electrode [12]. The

application of applied voltage prompts the formation of tiny hydrogen and oxygen bubbles at the tool electrode and auxiliary electrode, respectively. These tiny bubbles amalgamate with each other physically and result in the formation of bigger size bubbles. It leads to the formation of gas film at the tool surrounding area and constricts the current flow. Thus, a spark is generated owing to the electric breakdown of the gas film. The electric field generated inside the gas film is of order 10^6 - 10^8V/m [13]. Generally, sparks occur at a voltage larger than the critical voltage (Typically 30V). However, it depends on the tool shape and electrolyte concentration. A further increase in voltage leads to an increase in the formation rate of bubbles. It increases the current densities. The work material is then placed underneath the tool electrode and material removal occurs due to thermal energy given by the sparks. Chemical etching also results in the erosion of the material.

Basak and Ghosh [14] developed a model for comprehending the spark mechanism. They proposed that critical voltage and current are required to initiate the spark in the ECDM process. El-Haddad et al. [15] predicted the current and voltage values for stable gas film formation at the tool vicinity area. Wuthrich et al. [16] successfully produced micro-holes on non-conductive materials and emphasized that gas film is the key determinant in controlling the machining features. Bhattacharyya et al. [17] elaborated on the removal phenomena in the ECDM process and highlighted the areas for improving the machining performance. Jain et al. [18] demonstrated an improvement in the machining depth of alumina material when machined using abrasive cutting tools with ECDM. Wuthrich [19, 20] made monumental contributions in the field of the ECDM process and highlighted the mechanism of the different tool feed system. Gravity assisted tool feed system results in the formation of high thermal cracks due to the physical contact of the tool electrode with the work material. A constant tool feed method exhibits better geometrical accuracies in terms of hole circularity and heat-affected zone. However, feed rate higher than material removal results in the breakage of the tool electrode. Wuthrich et al. [21] described the possibility of developing a tool feed that works on actual machining conditions. It is referred to as a closed-loop machining or adaptive machining. The adaptive tool feed system is used in this present investigation (Section 4.1). Yasuda et al. [22] analyzed the amalgamation process of the tiny bubbles inside the electrolyte. They concluded that the presence of bubbles in the inter-electrode area substantially affects the inter-electrode resistance. It results in the change of the current densities within the circuit.

A pioneering study on the evaluation of applied voltage, electrolyte concentration, tool shape, tool feed on MRR was reported by several authors [23-25]. Goud et al. [26] reported that with the increasing electrolyte concentration from 20 wt% to 30 wt%, the material removal rate increases from 0.1515mm^3/min to 0.5556mm^3/min during micro-channelling on the quartz work material. An increase in electrolyte concentration enhances the ion's mobility that results in the higher formation of hydrogen bubbles. As a result, high intensity of sparks occurs [27]. Gautam and Jain [25] studied the process capabilities of the ECDM process using various tool kinematics.

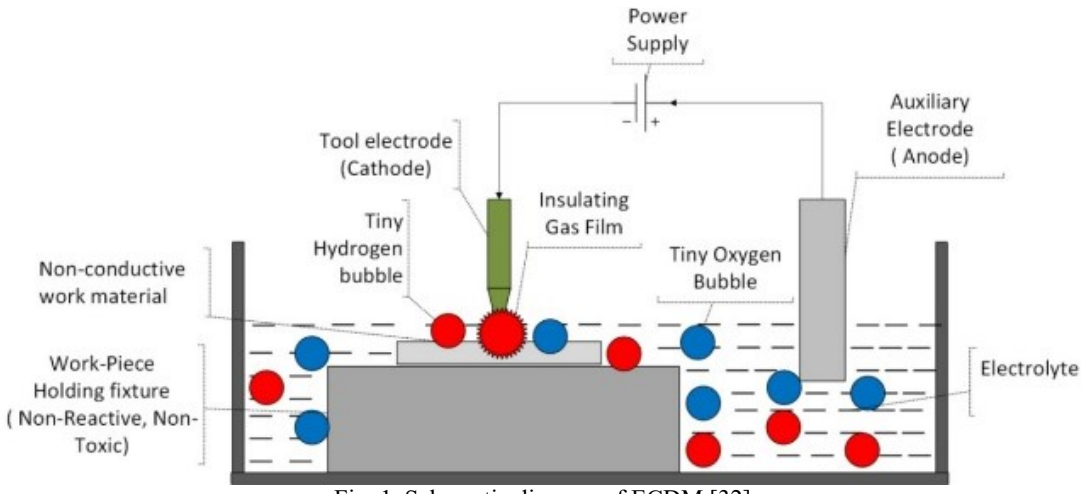

Fig. 1. Schematic diagram of ECDM [32]

Zheng et al. [28] described an improvement in hole taperness with the application flat sidewalls. Various ECDM variants and hybrids were presented for enhancing the ECDM machining performance [29-32]. Overall hole quality in terms of circularity, taperness and aspect ratio was improved by utilizing the different mechanisms such as tool rotation [33], tool vibration [32], magnetic field assistance [34], etc.

Apart from experimental studies, various analytical studies were also reported to study the simulation aspects of the ECDM process. Jain et al. [35] developed a finite element-based model to analyze the ECDM performance. The process is described as similar to the arc discharge valve theory. The model was based on uniform distribution of heat over the work material which was not practical. However, the effect of electrolyte concentration was not considered. Bhondwe et al. [36] built a two-dimensional axisymmetric model for predicting the material removal rate. The temperature plots were utilized to analyze the removal rate. A fair agreement was obtained between the predicted and experimental results. Wei et al. [37] also built a FEM based transient thermal model to simulate a single spark for discharge. Drilling depth was precited using temperature plots and results observed to be in accordance with the experimental results. Panda and Yadav [38] investigated the wire ECDM process with FEM based thermal model. The predicted results of material removal were found to be higher than the experimental results. It was due to an assumption of 100% ejection efficiency. Krotz et al. [39] investigated the heat-affected zone in the ECDM process by simulating a single spark in the 2D thermal model. It was concluded that HAZ is equivalent to the diameter of the arc spot.

Based on the available literature, it is concluded that the FEM based thermal model can be utilized to analyze the machining performance of the ECDM process. In this present investigation, FEM based transient thermal model is developed to analyze the material removal rate of glass, quartz, and alumina (Al_2O_3) materials. The developed model is validated by comparing it with previously reported simulation and experimental results. The effect of electrolyte concentrations on the material removal rate is also investigated for all work material.

2. THERMAL MODELLING

A transient thermal model is developed to predict the removal rate of different work material. Work material of dimensions *0.4 X 0.4 X 0.4*mm^3 was selected for developing the model and applying different boundary conditions as shown in Figure 2. Three different work materials were selected for comparing the material removal rate i.e., Soda-lime glass, quartz, and alumina. The crucial properties of these materials are highlighted in Table 1. A gaussian heat input was applied over the work material top surface in the spark region. Spark radius of 150μm was used in this study which was used by Bhondwe and other authors [36, 40-42]. The simulations were performed using ANSYS software.

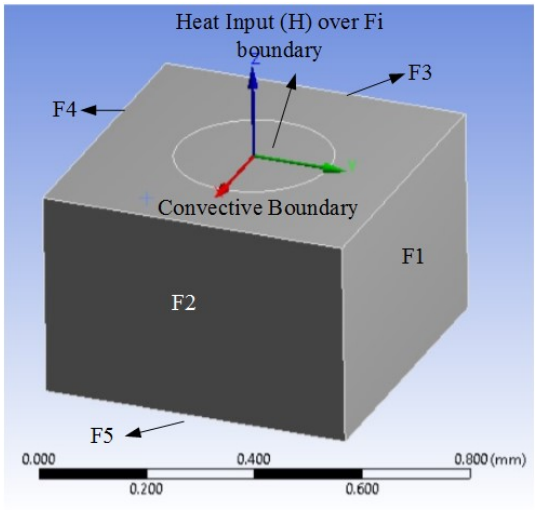

Fig. 2. A developed model with boundaries

Table 1. Work material properties used for FEM analysis [36,40]

Property	Soda-lime	Quartz	Alumina (Al_2O_3)
Thermal Conductivity (W/mK)	1.6	1.4	26
Heat Capacity (J/kgK)	670	733	875
Melting temperature (K)	1673	1943	2100
Room temperature (K)	298	298	298
Density (Kg/m^3)	2100	2650	3900
Convective coefficient (W/m^{2}K)	10000	10000	10000

2.1 Assumptions

The following assumptions were made for developing a FEM based thermal model to analyze the removal rate of different work materials.

1. Work material properties are assumed to be isotropic and homogeneous in nature.
2. Only one spark at a time is assumed.
3. Gaussian heat distribution is assumed within the spark region.
4. A spark duration of 100 μs is assumed for a single spark.
5. The formation of the crater is assumed to be dome-shaped.
6. Energy transference (E_p) to the work material is assumed to be fractional. E_p = 20% is used in this model [36].
7. Machining conditions during the ECDM process is assumed to be constant.
8. Effect of tool wear, drop of electrolyte level and recast layer formation is neglected.

2.2 Boundary Conditions

1. The work material temperature (K)at an initial time i.e., t=0 is assumed to be at room temperature (T).
2. A total heat input (H) is received at the circular boundary (F_i) over the work material top surface.

Gaussian heat distribution is assumed within the spark region and expression is given as, equation (1):

$$H = \frac{4.45 E_p VI}{\text{Area of Spark}} \exp\left\{-4.5\left\{\left(\frac{r_x}{R}\right)^2 + \left(\frac{r_y}{R}\right)^2\right\}\right\} \quad (1)$$

where (V) is the voltage, (I) is the current, (r_x, r_y) is the radial distance, (R) is the spark radius. Energy transference (Ep) of 20% is applied in this model by citing the study of Basak and Ghosh [14].

3. All other boundaries (F1, F2, F3, F4 & F5) are perfectly insulated. No heat transfer takes place across these boundaries, equation (2).

$$\frac{\partial T}{\partial n} = 0, t \geq 0 \quad (2)$$

4.The remaining boundary of the top surface releases heat into the atmosphere through convection. It is given as equation (3):

$$C = h(T - T_0) \quad (3)$$

where h is a convective coefficient, T is work material temperature, T_0 is room temperature.

5. The current values are computed by utilizing the derived equation $I = 3.2323\ X\ 10^{-5}C^3 - 0.0027056C^2 + 0.091378C + 0.71429$, given by the Bhondwe model. It is a function of electrolyte concentration (C) and used by other authors [40, 41].

2.3 Material removal

The estimation of material removal is obtained by utilizing the temperature plots of the work material. Different work material produces different temperature plots that further results in different material removal. In this present investigation, material removal is estimated for glass, quartz, and Alumina.

It is a known fact that material removal is directly related to the temperature of the work material. Thus, material removal is assumed to have occurred when work material temperature becomes higher than the work material melting temperature. It is expressed as, equation (4):

$$T > T_m \quad (4)$$

The identification of the melting temperature in isothermal temperature planes provides the coordinates of intercepts as shown in Figure 3. These coordinates are then used to calculate the material removal due to single spark and mathematically expressed as, equation (5):

$$V_m = \iiint r_o z_0 \theta \, dr dz d\theta = \frac{2}{3}\pi r_o^2 z_o \quad (5)$$

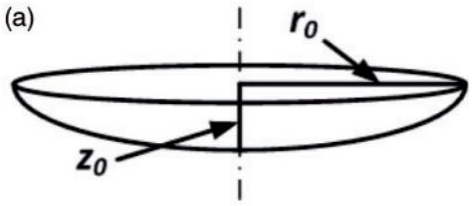

Fig. 3. An isothermal curve with intercepts [43]

where r_o and z_o are the axis's intercepts; V_m is the removed volume from the work material. The shape of the volume removed is assumed to be hemisphere under the spark region [36, 40]. The total volume removed is estimated by calculating the total number of sparks in one minute, equation (6).

$$V_T = V_m X \ number\ of\ sparks\ per\ unit\ time \quad (6)$$

The sparks produce impressions at the entrance of the hole entrance which exhibits the dome-shaped nature of the crater as shown in Figure 4. The net removal of material in mg/min is obtained by multiplying it with a work material density (ρ), equation (7).

$$MRR = V_T\ X\ \rho \quad (7)$$

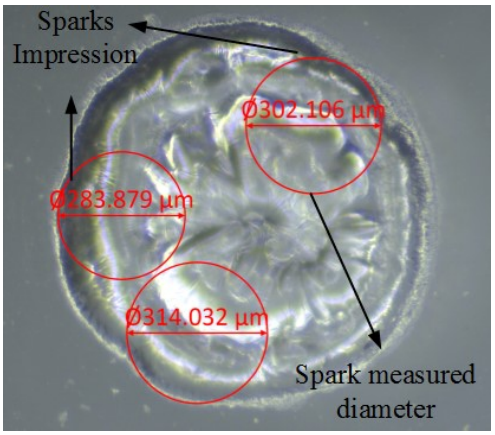

Fig. 4. Sparks impression at the micro-hole entrance

3. EXPERIMENTATION

The experiments are performed to validate the predicted results of the simulation study for all work materials. Soda-lime glass, quartz, and alumina were chosen as work material. The adaptive tool feed method is used for maintaining the constant machining gap between the work material and the tool electrode.

3.1 Adaptive tool feed

The developed experimental setup with adaptive tool feed control is shown in Figure 5. It uses the

application of a sensitive load cell which senses the physical contact between the tool and the work material. As soon as the physical contact is detected, the load cell produces a potential difference which acts as a signal to micro-controller.

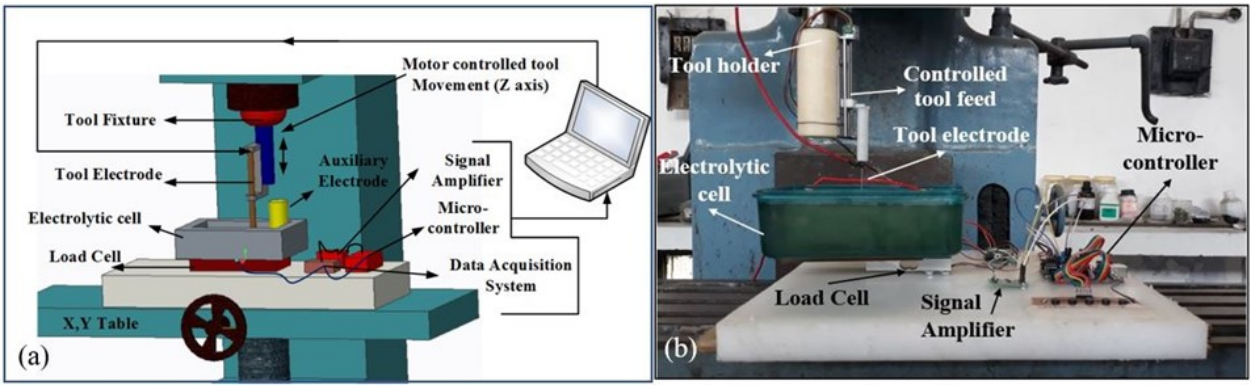

Fig.5. Adaptive tool feed system in the ECDM process (a) CAD model (b) Experimental Setup

The microcontroller was programmed to withdraw the tool in an upward direction to create the machining gap where the gas film is formed. It is unlike the gravity-assisted tool feed method where no sparks are generated beneath the tool electrode. Table 2 highlights the machining conditions used in experimental studies.

3.2 Material removal measurement

The material removal rate (MRR) is computed as the difference of the work material's weight before and after micro-drilling per unit time. The expression for MRR is given as, equation (8):

$$MRR = \left(wt_b - wt_a\right)/t \tag{8}$$

where wt_b = weight of work material before micro-drilling (g), wt_a = weight of glasswork material after the micro-drilling operation (g), and t = time in minutes. An average of three measurements was considered.

Table 2. Machining Conditions.

Parameter	Value
Applied Voltage	40V-60V
Electrolyte	NaOH
Electrolyte Concentration	20%- 60% (%wt. /V.)
Tool Feed Rate	3 mm/min
Tool Immersion depth	1mm (Approx.)
Tool Material	Tungsten Carbide
Tool Shape	Cylindrical
Tool Size	1000 μm
Inter Electrode Gap	40 mm
Machining time	1 min

4. RESULTS AND DISCUSSION

4.1 Model Validations

The thermal model is developed to investigate the material removal rate of different work materials. The material removal rate is analyzed by obtaining the plots of temperature distributions. The process of thermal modeling involves the meshing of the model trailed by the solution. The meshing of the model is performed to achieve accurate results. A hex dominant method with volume type heat transfer was used to perform the meshing analysis. The spark region was refined further to achieve more accuracy in the results. The meshed model is shown in Figure 6.

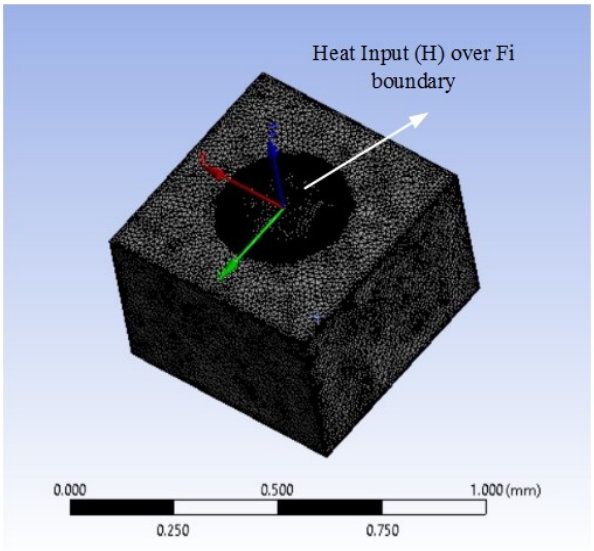

Fig. 6. Meshed Model

The temperature plots distribution within the work material is shown in Figure 7.

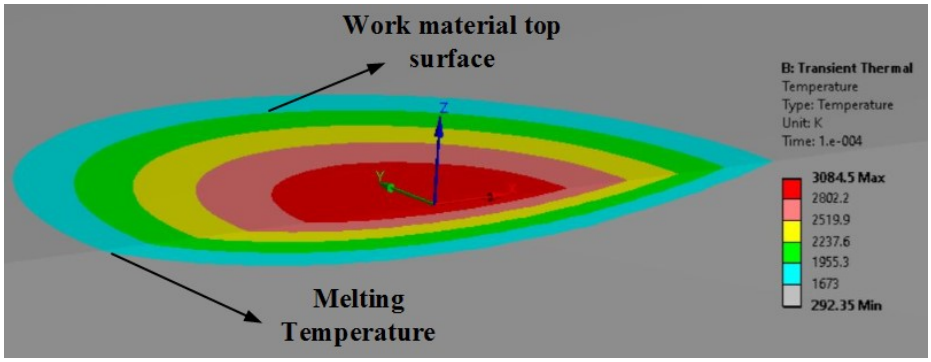

Fig.7. Temperature distributions within the soda-lime glass work material at 20 wt% and 45 V

The developed model was compared with the previously developed model given by Goud et al. [40]. The temperature plots over the work material surface in a radial direction are compared for soda-lime glass using NaOH electrolyte as described in Figure 8. It was found that the trend of temperature variation is similar. However, some differences in the temperature values were also observed. It was accounted for by the fact that the Goud model is based on a three-dimensional spark region while the current model is based on a two-dimensional spark region.

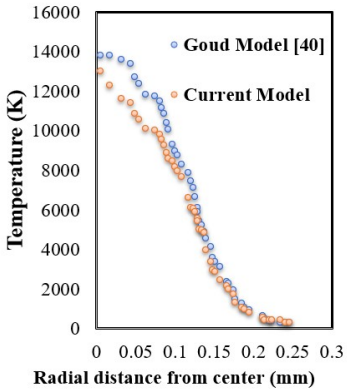

Fig.8. Temperature distribution in a radial direction at 20 wt% NaOH concentration

For assessing the efficacy of the current thermal model, a comparison of MRR for soda-lime glass was made with the (i) existing simulated results, (ii) existing experimental results and (iii) Present experimental results. Figure 9 (a) shows the comparison of MRR predicted in this model with the previously simulated and experimental results. It was seen that MRR variations are found to be similar. However, a difference in MRR was observed when compared with the Bhondwe [36] and Goud model [40]. It was expedited on the fact that the Bhondwe model evaluated temperature plots for some portion of the work material and integrated it for the full work material. In the present model, the temperature plots are calculated for a full portion of the work material. Also, Bhondwe utilized pulse voltage supply that also leads to a difference in MRR values.

Moreover, MRR predicted in this model found to be in fair agreement with the experimental results. The correlation coefficient (R^2) is calculated as 0.99. A maximum difference of 1.33mg/min in MRR was observed between these two owing to different assumptions made during the simulation process i.e., Energy transference (E_p), Spark radius, etc.

4.2 Material removal validation

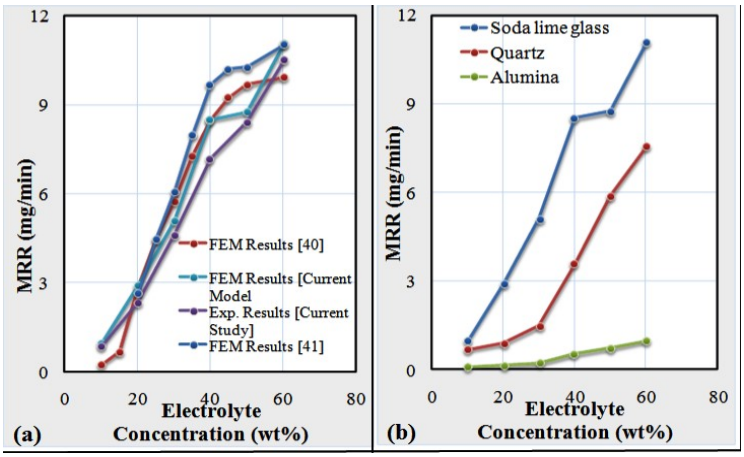

Fig. 9. MRR variation at different NaOH electrolyte concentration (a) Comparison with previous FEM results (b) Different work materials

4.3 Material removal comparison of different work materials

The material removal rate (MRR) of different work materials was compared to analyze the machining performance of ECDM. Figure 9 (b) shows the MRR variation for all three different work materials at different NaOH electrolyte concentrations. It was analyzed from the figure that soda-lime glass exhibits maximum MRR in comparison to quartz and alumina. The difference in material removal rate is accounted for the fact of different work material properties. Alumina found to be laboriously removed with the ECDM process during a micro-hole drilling operation. It is because that alumina is harder than soda-lime glass and quartz. Thus, it is difficult to etch and remove material from alumina.

Figure 10 shows the temperature distributions of soda-lime glass, quartz and alumina materials at 20 wt% and 45V. It is depicted from the figure that the peak temperature was obtained with soda-lime glass. An increase of 516.8K in temperature was found in a soda-lime glass when compared to alumina's work material. An increase of 3.53 and 10.13 in MRR (mg/min) was found in a soda-lime glass when compared to quartz and alumina at 60 wt% NaOH concentration.

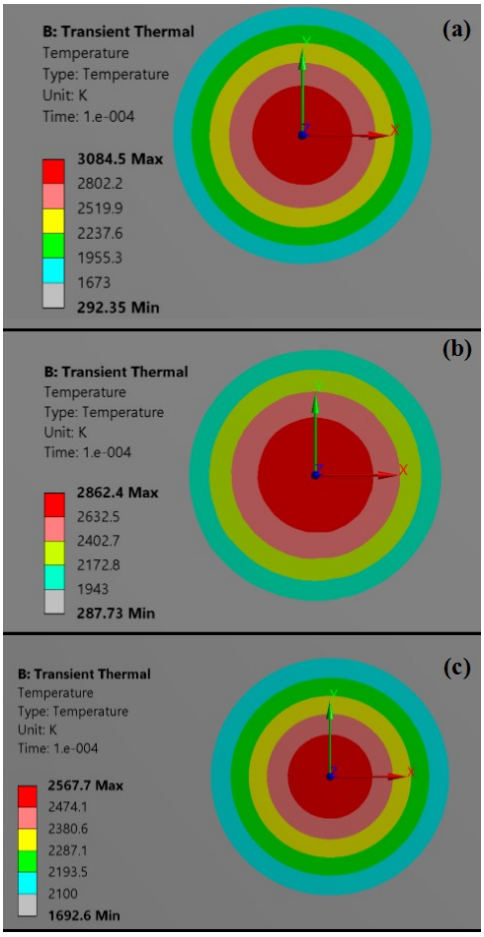

Fig.10. Temperature distributions (a) Soda-lime glass (b) Quartz (c) Alumina at 20 wt% NaOH concentration

4.4 Effect of electrolyte concentration on MRR

Figure 9 shows the plot of MRR variation at different NaOH concentrations. An increase in MRR was found with an increase in electrolyte concentration. Any increase in electrolyte concentration leads to an increase in ion mobility which further improves the electrolyte conductivity. With the increase in electrolyte concentration, the development rate of hydrogen bubbles increases which accelerates the gas film formation. Hence, high intensity of sparks occurs over the work material. As a result, higher MRR was obtained. There is an increase in MRR for all the materials.

Soda-lime glass exhibits a higher MRR at 60 wt% when compared to quartz and alumina. An increase of 2.34, 1.68 and 0.245 in MRR (mg/min) was observed in soda-lime, quartz and alumina respectively when electrolyte concentration increases from 50 wt% to 60 wt%.

4.5 Effect of applied voltage on MRR

Figure 11 shows the MRR variation of at different applied voltage. The applied voltage varies from 40 V to 60V at an interval of 5V. It was seen that MRR improves with the increase in applied voltage for all work materials. But soda-lime glass exhibits a higher increase in MRR when compared to quartz and alumina. An increase in MRR is explained by the fact that increasing applied voltage results in the rapid formation of tiny hydrogen bubbles. It produces rapid gas film and as a result, enhances the spark intensity. Hence, high MRR is obtained. An increase of 5.50mg/min in MRR was obtained in a soda-lime glass when applied voltage increases from 40V to 60V. However, an increase of 2.03mg/min and 5.71mg/min in MRR was obtained in a soda-lime glass when compared to quartz and alumina at 60V.

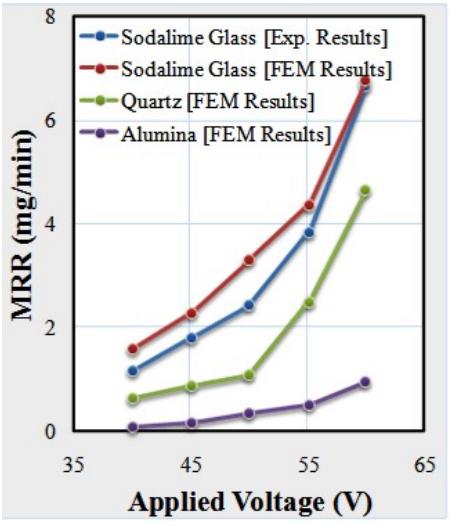

Fig.11. MRR comparison at the different applied voltage for different work materials, 20 wt% NaOH

4.6. Analysis of drilled micro-holes

The microscopic images of the drilled micro-holes were obtained to analyze the state of holes. Hole entrance diameter and cracks were observed. Figure 12 shows the micro-hole entrance diameter drilled at 20 wt% and 45V. Maximum hole entrance diameter was observed in a soda-lime glass when compared to quartz and alumina. Soda-lime glass exhibits a lower melting temperature of 1673K compared to quartz (1943K) and alumina (2100K). It makes soda-lime glass to remove and etch easily. The heat affected Zone and redeposited material is clearly visible at the micro-hole edges. Figure 12 also shows the morphology of the drilled micro-hole obtained through thermal erosion and chemical dissolution.

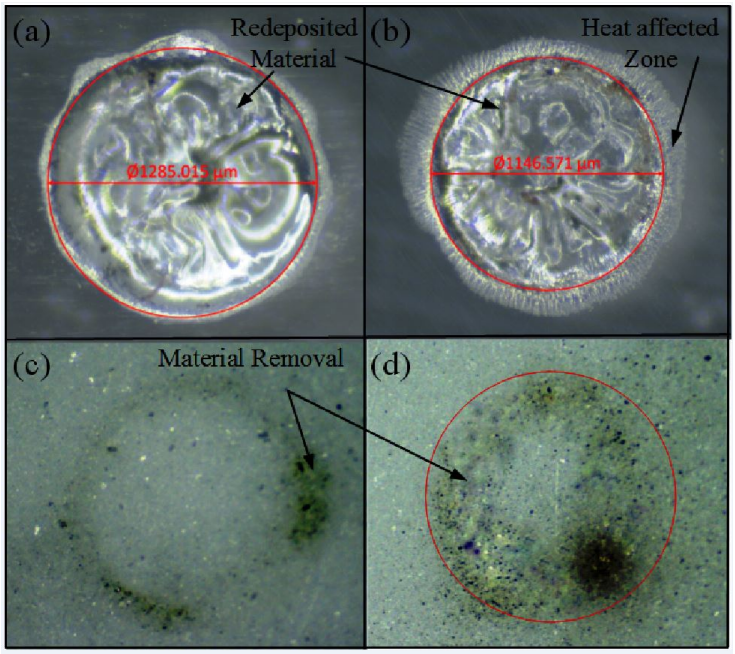

Fig.12. Microscopic images of micro-holes (a) Soda lime glass (b) Quartz (c) & (d) Alumina

5. CONCLUSIONS

In this present article, the machining performance of the soda-lime glass, quartz, and alumina in terms of material removal was analyzed using FEM based thermal model. The major conclusions are given below:

- The developed FEM based thermal model displays good agreement with the existing simulation models.
- An increase of 516.8K in peak temperature was found in a soda-lime glass when compared to alumina's work material.
- The predicted results are found to be in accordance with the existing FEM and experimental results. A fair agreement was obtained between the predicted MRR and experimental MRR with a correlation coefficient (R^2) of 0.99.
- An improvement in MRR was observed with the increase in electrolyte concentration and applied voltage for all work materials. An increase in MRR for soda-lime glass is higher when compared to quartz and alumina work materials. NaOH produces higher MRR of 6.78mg/min at 60V.

Alumina is harder in comparison to other materials and possesses a high melting temperature of 2100 K. As a result, low material removal was reported in alumina.

6. NOMENCLATURE

h: Convective Heat Coefficient (W/m^2K)
ρ: Density (kg/m^3)
c: Specific Heat Capacity (J/kgK)
k: Thermal Conductivity (W/mK)
H: Internal Heat generation (W/m^2)
E_p: Energy Transference
V: Applied Voltage
I: Current
C: Convective heat transfer (W/m^2)
h: Convective coefficient
T: Work material temperature (K)
T_0: Initial Temperature (K)
T_m: Melting temperature (K)
R: Spark Radius (µm)

7. REFERENCES

1. Sindhu, D., Thakur, L., Chandna, P., (2019). *Multi-objective Optimization of Rotary Ultrasonic Machining Parameters for Quartz Glass Using Taguchi-Grey Relational Analysis (GRA).* Silicon, **11**, 2033–2044, doi: 10.1007/s12633-018-0019-6.

2. Bindu Madhavi, J., Hiremath, S.S. (2019). *Machining and Characterization of Channels and Textures on Quartz Glass Using μ-ECDM Process*. Silicon, **11**, 2919–2931. doi: 10.1007/s12633-019-0083-6.
3. Dam, H., Quist, P., Schreiber, M.P., (1995). *Productivity surface quality & tolerances in ultrasonic machining of ceramics*. Journal of Material Processing Technology, **51**, 358-368.
4. Zhang, J. H., Lee, T. C., Lau W. S., (1997). *Study on the electro-discharge machining of a hot pressed aluminum oxide-based ceramic*. J. Mater. Process. Technol., **63**, 908-912.
5. Yilbas, B.S., Akhtar, S.S., Karatas, C., (2016). *Laser machining of different diameter holes in alumina ceramic: Thermal stress analysis*, Mach. Sci. Tech., **20**(3), 349-367. doi: 10.1080/10910344.2016.1191024
6. Singh, R., Singhal, S., (2017). *Investigation of machining characteristics in rotary ultrasonic machining of alumina ceramic*, Mater. Manuf. Process., **32**(3), 309-326. doi: 10.1080/10426914.2016.1176190
7. Zaripov, A.A. and Ashurov, K.B., (2011). *Electrical discharge machining of nonconductive materials,* Surf. Engin. Appl. Electrochem., **47**(3), 197-200. doi: 10.3103/S1068375511030021
8. Mahamani, A. and Chakravarthy, V.V.A., (2017). *Investigation on laser drilling of AA6061-TiB_2/ZrB_2 in situ composites*, Mater. Manuf. Process., **32**(15), 1700-1706. doi: 10.1080/10426914.2016.1244836
9. Cao, X. D., Kim, B. K. and Chu, C. N. , (2009). *Micro-structuring of glass with features less than 100μm by electrochemical discharge machining*, Prec. Eng., **33**, 459-465.
10. Elhami, S. and Razfar, M. R. (2020). *Numerical and experimental study of discharge mechanism in the electrochemical discharge machining process*. J. Manuf. Process., **50**, 192-203, doi: 10.1016/j. jmapro.2019.12.040.
11. Kurafuji, H., Suda, K. (1968). *Electrical discharge drilling of glass*. Ann CIRP., **16**, 415–419.
12. Wüthrich, R., Comninellis, C.H. and Bleuler, H., (2005). *Bubble evolution on vertical electrodes under extreme current densities*, Electrochim. Acta., **50**, 242-246.
13. Wüthrich, R. and Fascio, V. , (2005). *Machining of non-conducting materials using ECDM phenomenon - an Overview*, Int. J. Mach. Tools Manuf., **45**, 1095-1108.
14. Basak, I. and Ghosh, A., (1997). *Mechanism of material removal in electro- chemical discharge machining: a theoretical model and experimental verification.* J. Mater. Process. Technol., **71**, 350–359.
15. El-Haddad, R. and Wüthrich, R., (2010). *A mechanistic model of the gas film dynamics during the electrochemical discharge phenomenon*, J. Appl. Electrochem., **40**, 1853–1858.
16. Wuthrich, R., Hof, L.A., Lal, A., Fujisaki, K., Bleuler, H., Mandin P.H. and Picard, H., (2005). *Physical principles and miniaturization of spark assisted chemical engraving (SACE).* J. Micromech. Microeng., **15**, 268–275.
17. Bhattacharyya, B., Doloi, B.N., Sorkhel, S.K., (1999).*Experimental investigations into electrochemical discharge machining (ECDM) of non-conductive ceramic materials*. J. Mater. Process. Tech., **95**, 145-154.
18. Jain, V.K., Chak, S.K., (2002). *Electrochemical spark trepanning of alumina and quartz*. Mach. Sci. Technol., **4**(2), 277-290. doi: 10.1080/10940340008945710
19. Wuthrich, R., Spaelter, U., Wu Y., Bleuler, H. (2006). *A systematic characterization method for gravity-feed micro-hole drilling in glass with spark assisted chemical engraving (SACE).* J. Micromech. Microeng., **16**, 1891–1896.
20. Wuthrich, R., Hof, L. A. (2006). *The gas film in spark assisted chemical engraving SACE—a key element for micro-machining applications*. Int. J. Mach. Tools Manuf., **46**, 828–835. doi: 10.1016/ j.ijmachtools.2005.07.029
21. Wuthrich, R., Spaetler, U., Bleuler, H. (2006). *The current signal in spark-assisted chemical engraving SACE what does it tell us?* J. Micromech. Microeng., **16**, 779–785. doi: 10.1088/0960-1317/16/4/014
22. Hine, F., Yasuda, M., Nakamura, R. et al. (1975). *T Hydrodynamic studies of bubble effects on Ir-drops in a vertical rectangular cell.* J. Electrochem. Soc., **122**, 1185–90. doi: 10.1149/1.2134422
23. Saranya, S., Sankar, A.R. , (2015). *Effect of tool shape and tool feed rate on the machined profile of a quartz substrate using an electrochemical discharge machining process*, 2nd International Symposium on Physics and Technology of Sensors, ISPTS, pp.313-316.
24. Rajput, V.S., Goud, M.M., Suri, N. M., (2019). *Experimental investigation to improve the removal rate of material in ECDM process by utilizing different tool electrode shapes*, Int. J. Technical Innovation in Modern Engineering & Science (IJTIMES), **5**(2), 333–341.
25. Gautam, N., Jain, V.K. , (1998*). Experimental investigations into ECSD process using various tool kinematics*, Int. J. Mach. Tools Manuf., **38**, 15-27.
26. Goud, M.M. and sharma, A.K. , (2017). *On performance studies during micromachining of quartz glass using electrochemical discharge machining*, J. Mech. Sci. Technol., **31**, 1365-1372.
27. Rajput, V.S., Goud, M.M. and Suri, N. M. (2019). *Performance Analysis on the Effect of Different Electrolytes during Glass Micro Drilling Operation Using ECDM*. I-manager's Journal on Future Engineering and Technology, **14**(4), 5-13. doi: 10.26634/jfet.14.4.15788.

28. Zheng, Z.P., Su, H. C., Huang, F. Y., et al. (2007). *The tool geometrical shape and pulse-off time of pulse voltage effects in a Pyrex glass electrochemical discharge micro- drilling process*. J. Micromech. Microeng., **17**, 265–272. doi: 10.1088/0960-1317/17/2/012
29. Ladeesh, V. G., Manu, R. (2018). *Effect of machining parameters on edge-chipping during drilling of glass using grinding-aided electrochemical discharge machining (G-ECDM).* Adv. Manuf., **6**(2), 215–224. doi: 10.1007/s40436-017-0194-5
30. Paul, L., Antony, D. (2018) *Effect of tool diameter in ECDM process with powder mixed electrolyte*. IOP Conf Ser: Mater. Sci. Eng., **396**, 012070. doi: 10.1088/1757-899X/396/1/012070
31. Rusli, M., Furutani, K. (2012). *Performance of Micro-Hole Drilling by Ultrasonic-Assisted Electro-Chemical Discharge Machining*. Adv. Mat. Res., **445**, 865–870. doi: 10.4028/www.scientific.net/ AMR.445.865
32. Rajput, V.S., Goud, M.M., Suri, N. M. (2019). S*tudy on effective process parameters: toward the better comprehension of ECDM process*. Int.J. of Mod. Manufact. Technol., **XI**(2), 105-118.
33. Kumar, S., Dvivedi, A. (2018). *On effect of tool rotation on performance of rotary tool micro-ultrasonic machining.* Mater. Manuf. Process., **34**(5), 475-486. doi: 10.1080/10426914.2018.1512130
34. Cheng, C. P., Wu, K. L., Mai, C. C. et al. (2010). Magnetic *field-assisted electrochemical discharge machining.* J. Micromech. Microeng., **20**(7), doi: 10.1088/0960-1317/20/7/075019
35. Jain, V.K., Dixit, M., Pandey, M. (1999). *On the analysis of the electrochemical spark machining process*, Int. J. Mach. Tools Manuf., **39**, 165–186.
36. Bhondwe, K.L., Yadava V. and Kathiresan, G., (2006). *Finite element prediction of material removal rate due to electrochemical spark machining*, Int. J. Mach. Tool. Manuf., **46**, 1699–1706.
37. Wei, C., Xu, K., Ni, J. et al., (2011). *A finite element-based model for electrochemical discharge machining in discharge regime,* Int. J. Adv. Manuf. Technol., **54**, 987–995.
38. Panda, M. C. and Yadava, V. (2009). *Finite element prediction of material removal rate due to traveling wire electrochemical spark machining*. Int. J. Adv. Manuf. Technol., **45**, 506–520
39. Krotz, H., Raoul, R. R. and Wegener, K. (2013). *Experimental investigation and simulation of heat flux into metallic surfaces due to single discharges in micro-electrochemical arc machining micro-ECAM*. Int. J. Adv. Manuf. Technol., **68**, 1267–1275. doi: 10.1007/s00170-013-4918-9
40. Goud, M. M. and Sharma, A.K. (2017*). A three-dimensional finite element simulation approach to analyze material removal in electrochemical discharge machining*. Proc. IMechE Part C: J. Mechanical Engineering Science, **231**(13), 2417-2428. doi: 0954406216636167
41. Singh, D., Goud, M.M. (2018). *A 3D spark model to evaluate MRR in ECDM*. Journal of Advanced Manufacturing Systems, **18**(3), 435-446. doi: 10.1142/S0219686719500239.
42. Kulkarni, A., Sharan, R. and Lal, G.K. (2002). *An experimental study of discharge mechanism in electrochemical discharge machining*. Int. J. Mach. Tool Manuf., 42, 1121–1127.
43. Rajput, V.S., Goud, M.M., Suri, N. M. (2020) *Performance Analysis of ECDM Process Using Surfactant Mixed Electrolyte*. In: Sharma, V., Dixit, U., Sørby, K., Bhardwaj, A., Trehan, R. (eds) Manufacturing Engineering. Lecture Notes on Multidisciplinary Industrial Engineering. Springer, Singapore.

Received: April 11, 2020 / Accepted: June 15, 2020 / Paper available online: June 20, 2020